Supporting Information

Efficient afterglow across liquid, hydrogel, and solid states enabled by naphthalimide-doped polyacrylate copolymer emulsions under UV/visible excitation

Yan-Fang Zhuang[†a], Wei-Guang Chen[†b], Shi-Bo Yao[a], Lu-Yu Wang[a], Yu Chen[*a], and Hua-Ji Liu[*a]

[a] Department of Chemistry, School of Science, Tianjin University, Tianjin 300354, P. R. China

[b] Suzhou 3N Materials Technology Co., Ltd., Suzhou 215100, Jiangsu Province, P. R. China

Corresponding Authors

*E-mail: chenyu@tju.edu.cn (Yu Chen), liuhuaji@tju.edu.cn (Hua-Ji Liu)

[†] These authors contributed equally to this work.

Characterizations

^{1}H NMR spectra were recorded on a Bruker AVANCE III HD 400 MHz NMR spectrometer at 25 °C. High-resolution mass spectrometry (HRMS) spectra were recorded on Liquid Chromatography–High-Resolution Quadrupole Time-of-Flight Tandem Mass Spectrometer MicrOTOF-Q II. Fluorescence spectra were recorded on photoluminescence spectrometer (Tianjin Gangdong Sci & Tech Development Co., Ltd). Fluorescence lifetimes were measured on Edinburgh Instruments Fluorescence Spectrometer (FLS1000). The phosphorescence lifetime was measured on Hitachi F-7000. UV-vis spectrometry was performed on a Purkinje General (China) T6 UV/Vis Spectrophotometer. Differential scanning calorimetry (DSC) measurement was carried out on a Netzsch DSC 204 F1 Thermal Analysis System in the temperature range of -50 to 200 °C. The heating and cooling rate were set to be 10 °C/min and nitrogen flow rate was set to be 40 mL/min. Glass transition temperature (T_g) was determined as the median point of the transition recorded during the second heating process. Transmission electron microscopy (TEM) images were recorded by JEM-2100F.

Measurements of photoluminescent quantum yield: the total photoluminescence quantum yield (Φ_T) was measured using an integrating-sphere setup (FLS1000 spectrometer, Xe-lamp source, PMT-980 integrating-sphere detector). Prior to sample measurement, a blank scan was recorded under identical instrumental settings. The sample was then measured without altering any parameters. After background subtraction, Φ_T was calculated from the ratio of emitted photons (N^{em}) to absorbed photons (N^{abs}) according to Equation S1: $\Phi = N^{em}/N^{abs}$. To separate the contributions of fluorescence and phosphorescence, peak-deconvolution (fitting) analysis was

performed on the time-resolved and steady-state delayed emission spectra. This analysis allowed us to determine the relative spectral weight of the phosphorescent component. Combining this phosphorescence ratio with the independently measured Φ_T, the phosphorescence quantum yield (Φ_{Phos}) and, by difference, the fluorescence quantum yield (Φ_{FL}) were calculated.

Reagents and materials

2,3-Naphthalenedicarboxylic anhydride (99%) was purchased from Shang Hai Bide Pharmatech Ltd. and used directly. 2,4,6-Trimethylaniline (98%) was purchased from Tianjin Heowns Company and used directly. Methyl methacrylate (MMA), methyl acrylate (MA), ethyl acrylate (EA) and n-butyl acrylate (BA) were purchased from Tianjin Kewei Chemical Company and used directly. Sodium laureth sulfate (AES) was purchased from Shanghai Yuanye Bio-Technology Co., Ltd and used directly. Sodium dodecyl sulfate (SDS) and ammonium persulphate were purchased from Tianjin Jiang Tian Chemical Company and used directly. Other reagents were commercially available and used as received.

Synthesis of compounds

Five compounds *N*-Trimethylphenyl-2,3-naphthylimide (23NI-TMP), *N*-4-methylphenyl-2,3-naphthylimide (23NI-MP), *N*-phenyl-2,3-naphthylimide (23NI-Ph), *N*-Trimethylphenyl-1,8-naphthylimide (18NI-TMP) and *N*-Trimethylphenyl-1,4,5,8-naphthylimide (1458NI-TMP) were synthesized as below:

***N*-Trimethylphenyl-2,3-naphthylimide (23NI-TMP):** 2,3-Naphthalenedicarboxylic anhydride (0.5 g, 2.523 mmol), 2,4,6-Trimethylaniline (0.68 g, 5.029 mmol) and 0.1 mL of Triethylamine (TEA) were dissolved in 10 mL of *N,N*-dimethylformamide (DMF) and stirred at 130 °C for 12 h. After the reaction was completed, it was cooled and filtered, and the obtained crude product was washed by ethanol and then it was further purified on a silica gel column (eluent: 1:3 ratio of ethyl acetate to petroleum ether). After purification, the collected solid product after removal of eluent was placed in a vacuum drying oven at 60 °C for 48 h and the light brown powder was obtained (74%, yield). ^{1}H NMR (400 MHz, DMSO-*d*6) δ 8.65 (s, 2H), 8.32 (dd, J = 6.2, 3.4 Hz, 2H), 7.83 (dd, J = 6.2, 3.3 Hz, 2H), 7.06 (s, 2H), 2.31 (s, 3H), 2.05 (s, 6H). APCI (m/z): calcd for $C_{21}H_{17}NO_2$, 315.13. Found: 316.13.

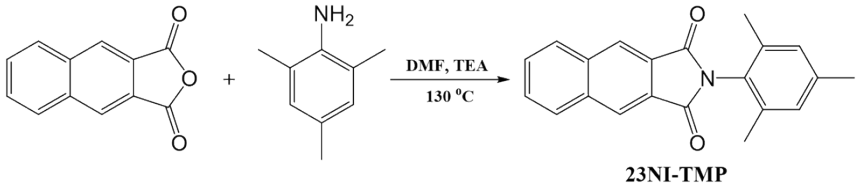

Scheme S1. Synthesis scheme for 23NI-TMP.

***N*-4-methylphenyl-2,3-naphthylimide (23NI-MP):** The same method as 23NI-TMP. Light brown solid, 67% yield. ^{1}H NMR (400 MHz, DMSO-*d*6) δ 8.60 (s, 2H), 8.30 (dd, J = 6.2, 3.4 Hz, 2H), 7.80 (dd, J = 6.2, 3.3 Hz, 2H), 7.35 (s, 4H), 2.38 (s, 3H).

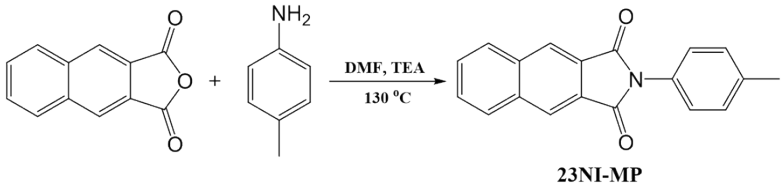

Scheme S2. Synthesis scheme for 23NI-MP.

***N*-phenyl-2,3-naphthylimide (23NI-Ph):** The same method as 23NI-TMP. Light brown solid, 73% yield. ^{1}H NMR (400 MHz, DMSO-*d*6) δ 8.63 (s, 2H), 8.31 (dd, J = 6.2, 3.4 Hz, 2H), 7.81 (dd, J = 6.2, 3.3 Hz, 2H), 7.56 (t, J = 7.6 Hz, 2H), 7.48 (dd, J = 16.4, 7.5 Hz, 3H).

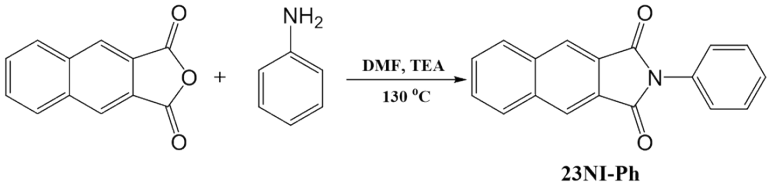

Scheme S3. Synthesis scheme for 23NI-Ph.

***N*-Trimethylphenyl-1,8-naphthylimide (18NI-TMP):** The same method as 23NI-TMP. Light brown solid, 64% yield. ^{1}H NMR (400 MHz, DMSO-*d*6) δ 8.54 (dd, J = 7.6, 3.8 Hz, 4H), 7.92 (t, J = 7.7 Hz, 2H), 7.02 (s, 2H), 2.30 (s, 3H), 1.96 (s, 6H). APCI (m/z): calcd for $C_{21}H_{17}NO_2$, 315.13. Found: 316.13.

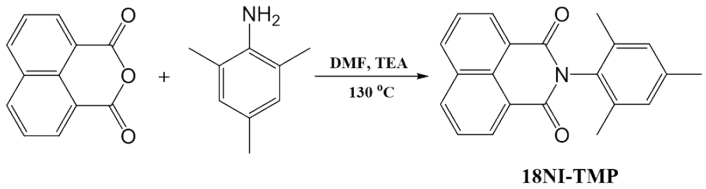

Scheme S4. Synthesis scheme for 18NI-TMP.

***N*-Trimethylphenyl-1,4,5,8-naphthylimide (1458NI-TMP):** The same method as 23NI-TMP. Brownish solid, 58% yield. ^{1}H NMR (400 MHz, DMSO-*d*6) δ 8.79 (s, 4H), 7.06 (s, 4H), 2.32 (s, 6H), 2.01 (s, 12H). APCI (m/z): calcd for $C_{32}H_{26}N_2O_4$, 502.57. Found: 503.20.

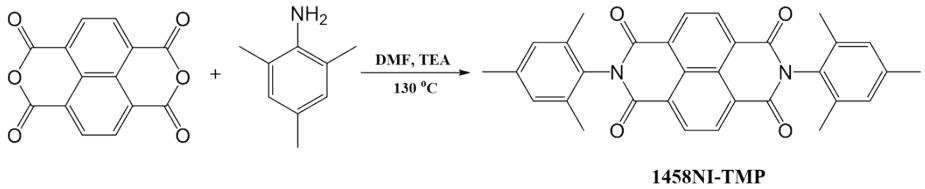

Scheme S5. Synthesis scheme for 1458NI-TMP.

General procedure of emulsion polymerization

Monomer (15 g), *N*-Trimethylphenyl-2,3-naphthylimide (23NI-TMP), sodium dodecyl sulfate (SDS) (0.025 g, 0.087 mmol) and sodium lauryl ether sulfate (AES) (102 d. nm: 0.3 g, 77 d. nm: 0.65 g, 67 d. nm: 1 g, 47 d. nm: 1.5 g) and 26 ml of water were mixed in a round-bottomed flask to prepare pre-emulsion. And then 1/3 of pre-emulsion was added to a four-necked round-bottomed flask (250 ml) equipped with a mechanical stirring bar, a cooling condenser, a thermometer and a dropping funnel. The pre-emulsion and 65 ^{o}C of water were stirred intensely for 10 min. The mixture was cooled down to room temperature and the 1/3 of aqueous solution of ammonium persulphate (0.7 g ammonium persulphate/1.5 g water) was added. The resulting mixture was stirred at 400 rpm for 3 h at 72 ^{o}C. And then the 1/3 of aqueous solution of ammonium persulphate was added and the reaction continued. The residue of pre-emulsion added to dropping funnel was dripped off within 2 h and the mixture was stirred at 300 rpm at 80 ^{o}C and then continued to react for 30 min. The remaining aqueous solution of ammonium persulphate was added and the resulting mixture was stirred for 3 h at 95 ^{o}C.

Computational Details

All calculations were carried out using the Gaussian 09 software. The ground-state geometry optimizations were performed with the B3LYP density functional method and the 6-31G* basis set. The excited-state properties were calculated using the time-dependent density functional theory (TD-DFT) method. Single-point TD calculations were carried out with the 6-31G basis set.

Results

Table S1. Summary of polymer-based long afterglow materials.

Chromophore	Matrix	τ_{Phos} (ms)	Φ_{phos} (%)	t_{ag} (s)	Ref.
2-(1*H*-benzo[*f*]indol-1-yl)-4-bromo-6-(9H-carbazol-9-yl)benzonitrile (CzBdBr)	PMMA	230	-	16	[1]
2,6-bis(1H-benzo[*f*]indol-1-yl)-4-bromobenzonitrile (2BdBr)	PMMA	110	-	20	[1]
Indolo[3,2,1-*jk*]carbazole-11-carbonitrile (ICz-pCN)	PMMA	2300	-	12	[2]
Indolo[3,2,1-*jk*]carbazole-10-carbonitrile (ICz-mCN)	PMMA	2110	-	12	[2]
Indolo[3,2,1-*jk*]carbazole-9-carbonitrile (ICz-oCN)	PMMA	~2500	-	12	[2]
3,6-dimethoxy-9H-carbazole	PMMA	2570 in N_2	21.1 in N_2	19	[3]
3-amino-4"-(diphenylamino)-2',5-dimethyl-[1,1':4',1"-terphenyl]-2,4-dicarbonitrile	PMMA	810	0.64	8	[4]
Phenanthrene	PMMA	1270	-	12	[5]
2-(7*H*-benzo[*c*]carbazol-7-yl)nicotinamide	PMMA	1300	-	-	[6]
Spiro[indolo[3,2,1-*de*]acridine-8,9'-xanthene]	PMMA	2133	10.3	16	[7]
Dimethyl 3,3'-(5,5'-dichloro-1*H*,1'*H*-[2,2'-bibenzo[*d*]imidazole]-1,1'-diyl)dipropionate	PMMA	265	-	3	[8]
4-(9*H*-carbazol-9-yl)benzonitrile	PMMA	525	3	7	[9]
Naphthalene	PMMA	950	-	8	[10]
(5,5-dioxido-10-(phenanthren-9-yl)-10*H*-phenothiazin-3-yl)(phenyl)methanone	PMMA	755	-	11	[11]
Truxene, coronene and hexabenzocoronene	PMMA/PC	2.65-5.50	3.87-11.87	20-50	[12]
N-Trimethylphenyl-2,3-naphthylimide	PMMA	2190	4.32	34	This work

Table S2. Energy levels, dominant excitations, and oscillator strength constants of the singlet and triplet excited states of 18NI-TMP.

Excited state	Dominant Excitations	Energy level (eV)	Oscillator strength, *f*
S_1	H→L	3.1060	0.0004
S_2	H-1→L	3.1982	0.0002
S_3	H→L+2	3.5269	0.0002
S_4	H-1→L+2	3.7720	0.2583
S_5	H→L+1	3.9523	0.0000
S_6	H-1→L+2	4.0795	0.0151
S_7	H-2→L	4.3942	0.0396
S_8	H-2→L+1	4.7507	0.0147
S_9	H-2→L+2	4.8448	0.0009
S_{10}	H-1→L+3	4.9565	0.0020
T_1	H-1→L	2.2858	0
T_2	H-1→L+2	3.0078	0
T_3	H→L+2	3.1961	0
T_4	H→L	3.2474	0
T_5	H→L+1	3.3378	0
T_6	H-1→L+1	3.5770	0
T_7	H-2→L	3.6044	0
T_8	H-1→L+2	3.6650	0
T_9	H-2→L+2	3.8789	0
T_{10}	H-2→L+1	4.4164	0

Table S3. Energy levels, dominant excitations, and oscillator strength constants of the singlet and triplet excited states of 1458NI-TMP.

Excited state	Dominant Excitations	Energy level (eV)	Oscillator strength, *f*
S_1	H→L	2.4465	0.0002
S_2	H-1→L	2.4572	0.0001
S_3	H→L+2	2.4940	0.0006
S_4	H-1→L+2	2.5073	0.0016
S_5	H→L+1	3.0307	0.0000
S_6	H-1→L+2	3.1691	0.0003
S_7	H-2→L	3.3383	0.4757
S_8	H-2→L+1	3.4702	0.0017
S_9	H-2→L+2	3.6435	0.0000
S_{10}	H-1→L+3	3.7666	0.0001
T_1	H-1→L	1.9543	0
T_2	H-1→L+2	2.4144	0
T_3	H→L+2	2.4286	0
T_4	H→L	2.4929	0
T_5	H→L+1	2.5064	0
T_6	H-1→L+1	2.7890	0
T_7	H-2→L	2.9030	0
T_8	H-1→L+2	2.9364	0
T_9	H-2→L+2	3.0202	0
T_{10}	H-2→L+1	3.1906	0

Table S4. Summary of photophysical properties of 23NI-TMP@ S-P(MMA/MA15) emulsion at room temperature

	τ_p (s, 520 nm)	Dyes-τ_{FL} (s)	Φ_{PRET} (%)	t_{ag}(s)
P(MMA/MA15)	1.95	-	-	29
S-P(MMA/MA15)	-	7.22×10^{-9}	-	-
0.04	1.94	1.85	0.5	24
0.40	1.66	1.38	14.9	21
1.90	1.12	0.87	42.6	11
3.80	0.86	0.60	55.9	11

Table S5. Summary of photophysical properties of 23NI-TMP@ S-P(MMA/MA15) film at room temperature

	τ_p (s, 520 nm)	Dyes-τ_{FL} (s)	Φ_{PRET} (%)	t_{ag}(s)
P(MMA/MA15)	2.19	-	-	30
S-P(MMA/MA15)				
0.04	1.40	1.30	36.1	26
0.40	1.25	1.21	42.9	23
1.90	0.84	0.77	61.6	12
3.80	0.52	0.41	76.3	8

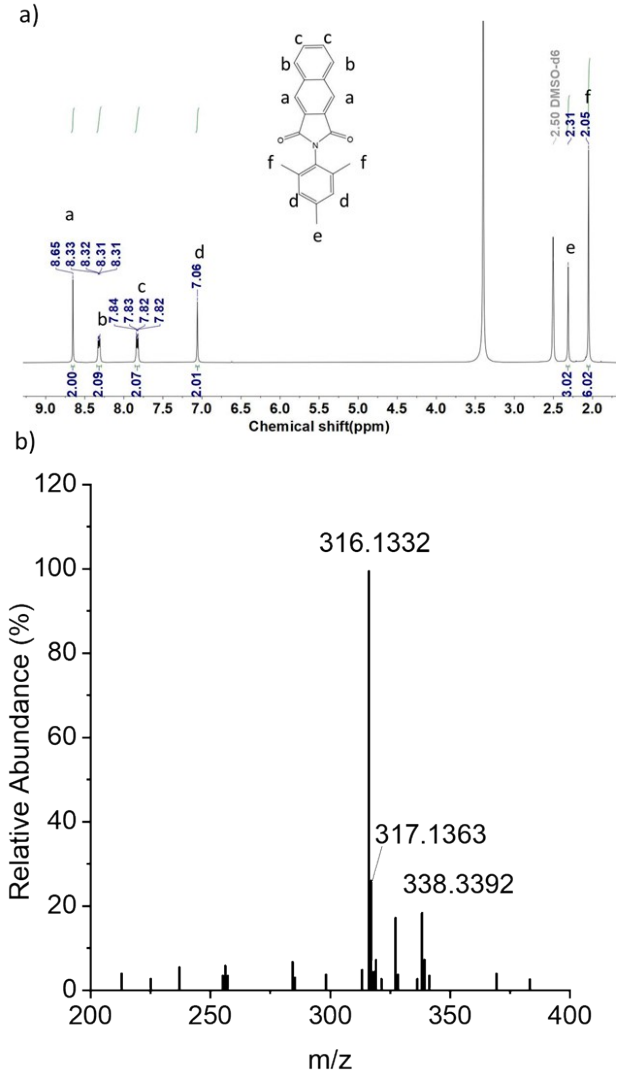

Fig. S1. a) ^{1}H NMR spectrum in DMSO-d_6 and b) HRMS spectrum of 23NI-TMP.

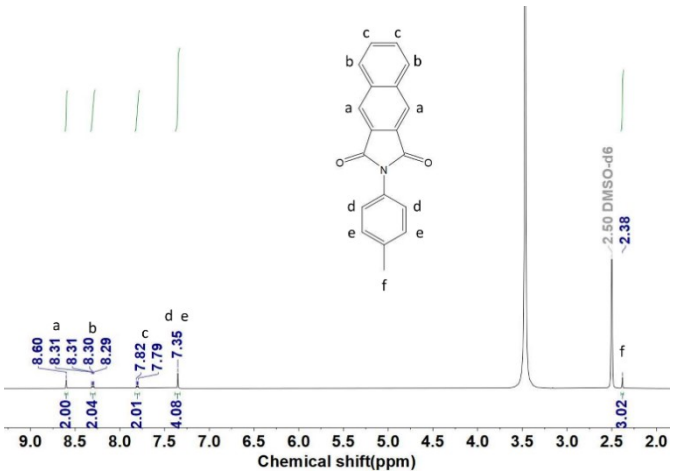

Fig. S2. ^{1}H NMR spectrum of 23NI-MP in DMSO-d_6.

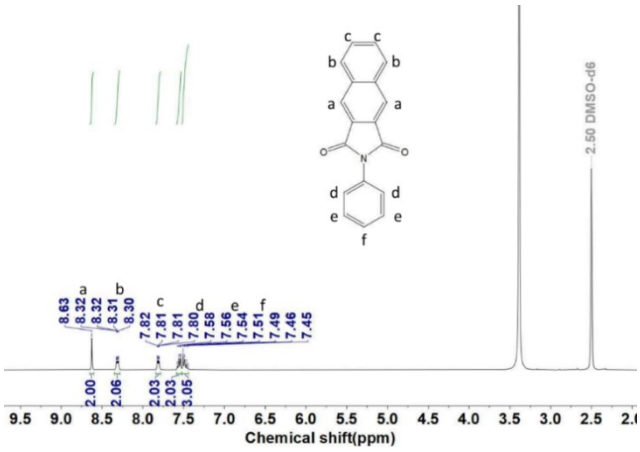

Fig. S3. [1]H NMR spectrum of 23NI-Ph in DMSO-d_6.

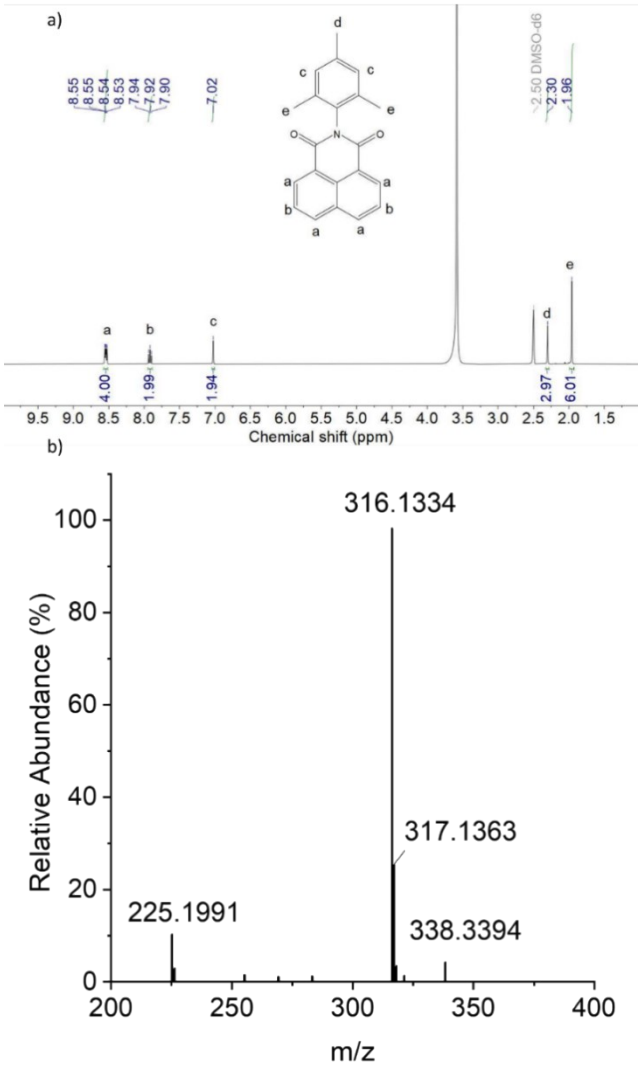

Fig. S4. a) [1]H NMR spectrum in DMSO-d_6 and b) HRMS spectrum of 18NI-TMP.

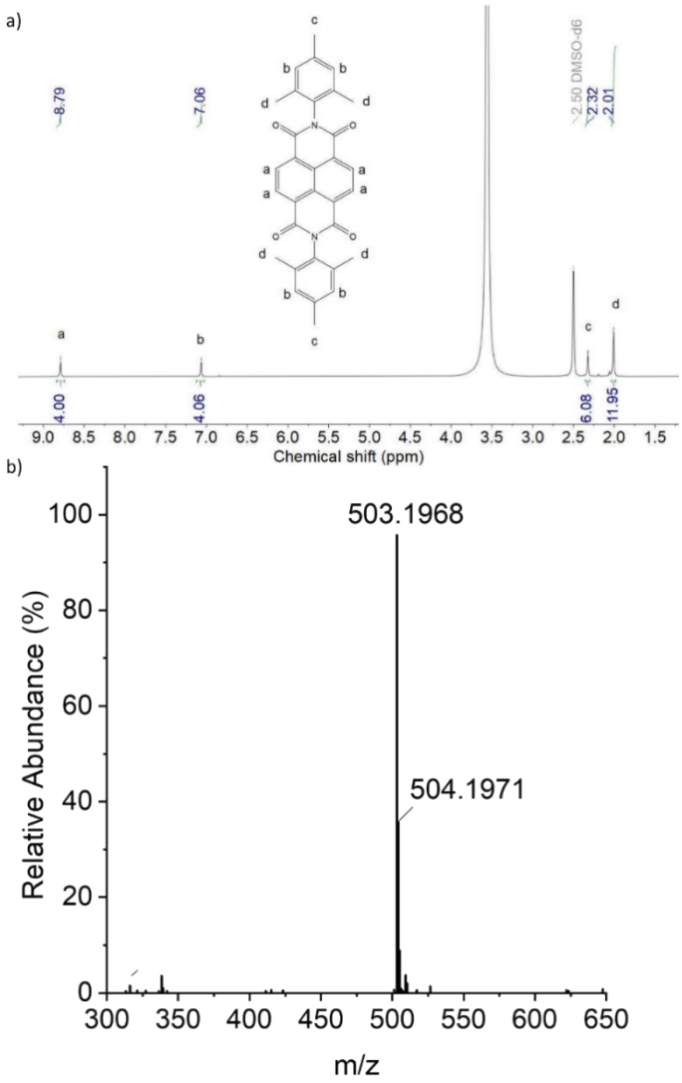

Fig. S5. a) ^{1}H NMR spectrum in DMSO-d_6 and b) HRMS spectrum of 1458NI-TMP.

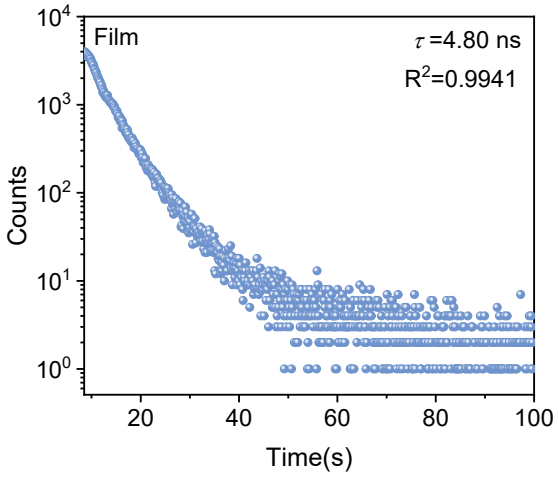

Fig. S6. Lifetime decay curves for the fluorescence emission peak of 23NI-TMP@P(MMA/MA).

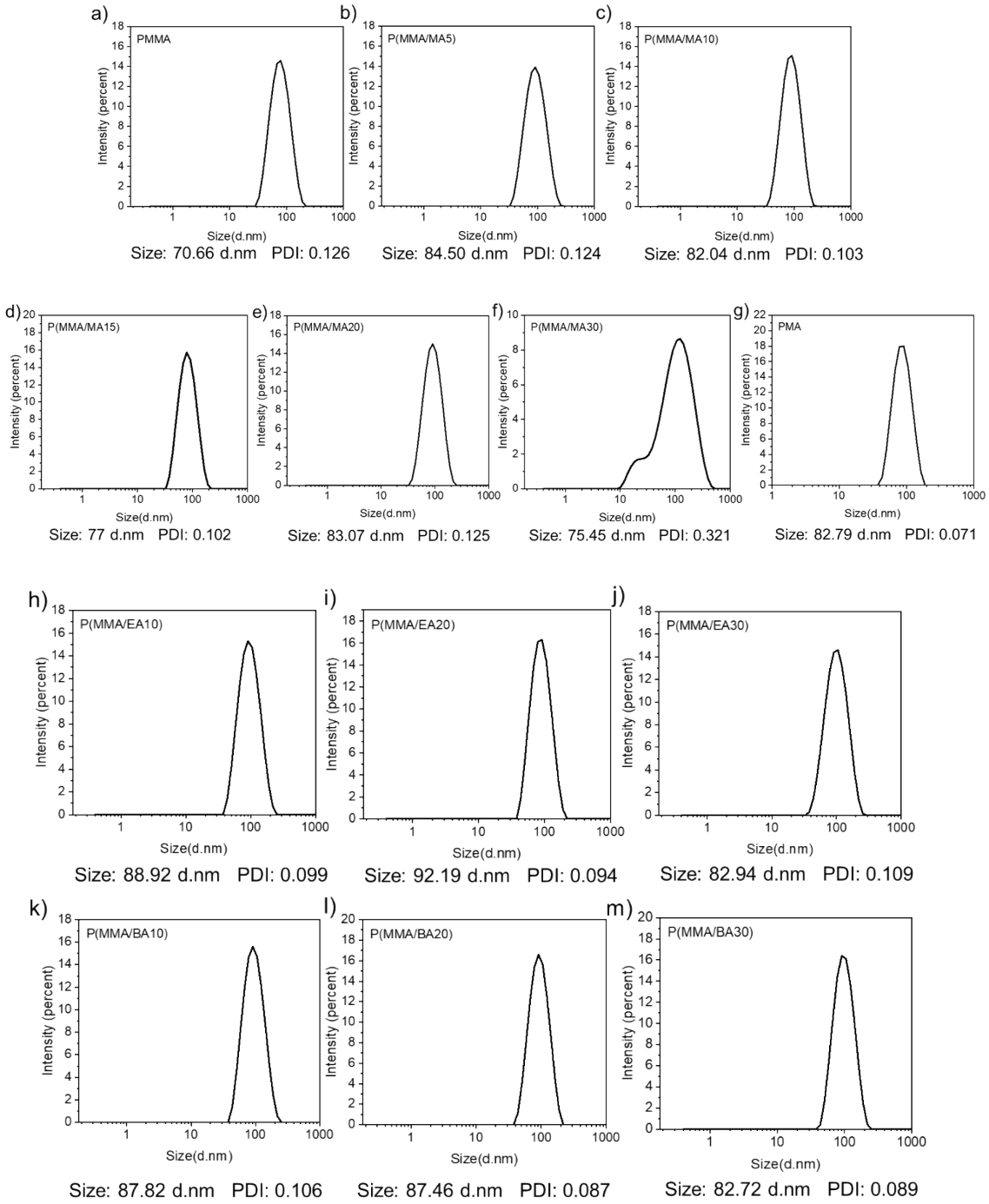

Fig. S7. Hydrodynamic diameter distributions of various polymer emulsions, as determined by dynamic light-scattering (DLS): a–g) PMMA, P(MMA/MA), and PMA emulsions; h–j) P(MMA/EA) emulsions; k–m) P(MMA/BA) emulsions.

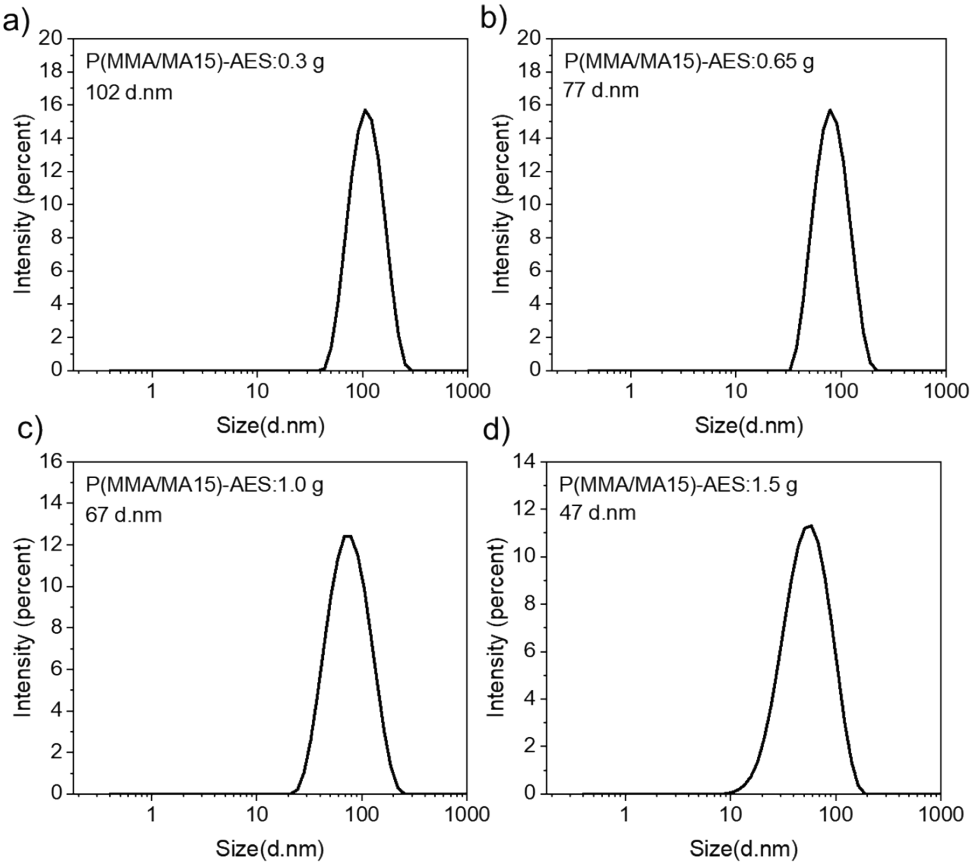

Fig. S8. Hydrodynamic diameter distributions of P(MMA/MA15) emulsions prepared with four different amounts of AES, as measured by dynamic light-scattering (DLS).

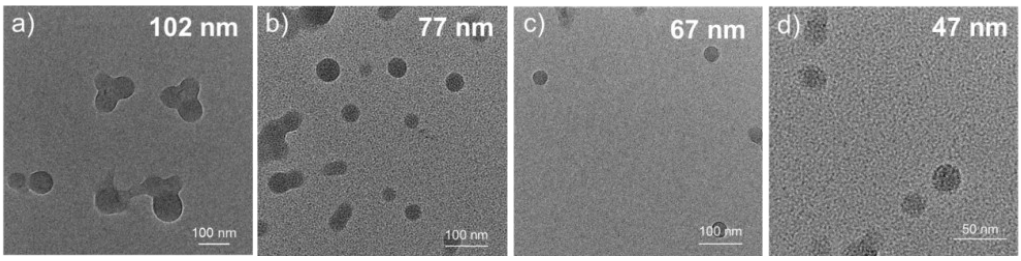

Fig. S9. TEM images of P(MMA/MA15) with different hydrodynamic diameters.

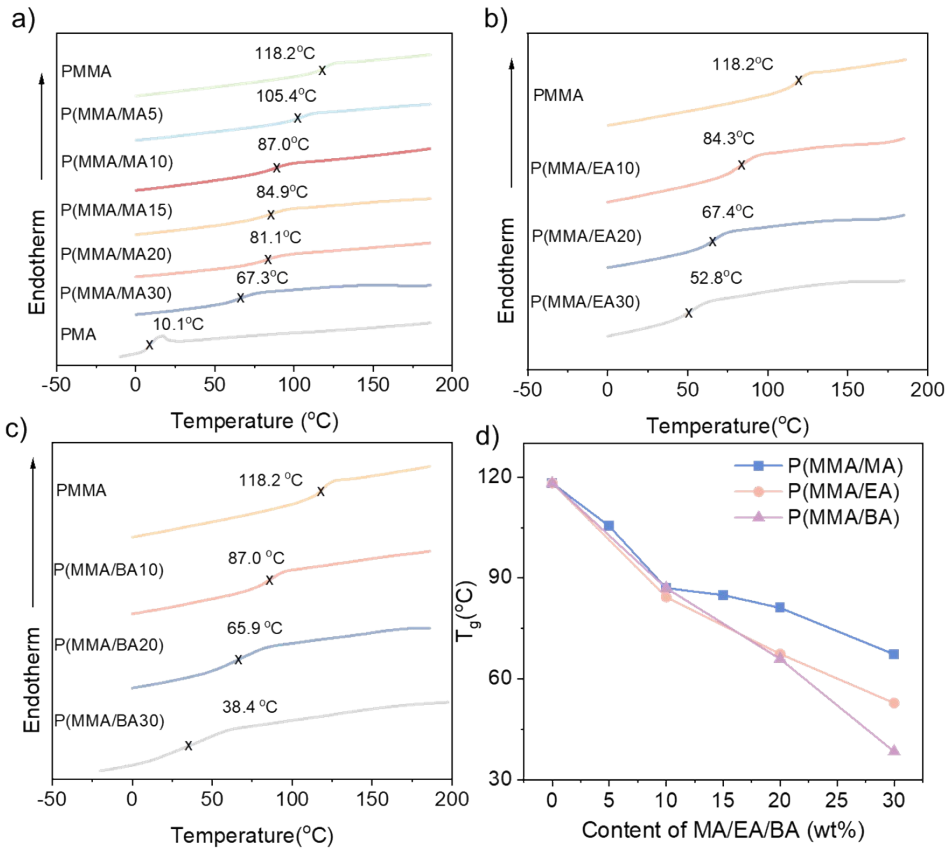

Fig. S10. Second-heating DSC thermograms of a) P(MMA/MA), b) P(MMA/EA), and c) P(MMA/BA) copolymers; d) corresponding changes in glass transition temperature (T_g).

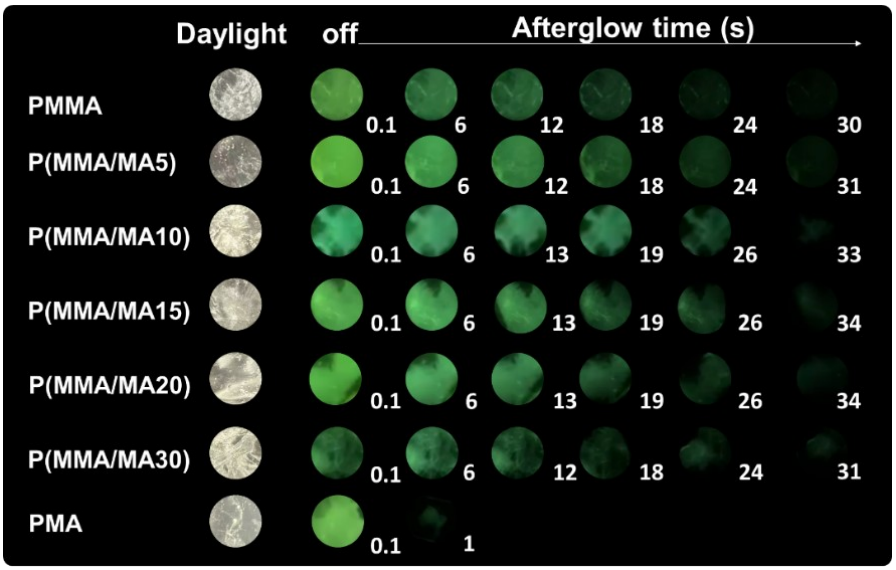

Fig. S11. Afterglow photos of P(MMA/MA) films (UV lamp excitation power is 10 mW/cm²).

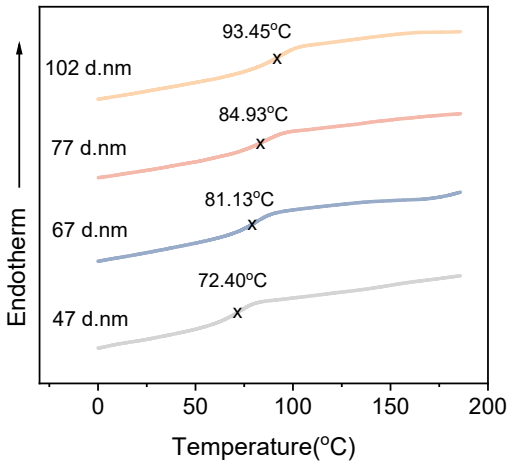

Fig. S12. Second-heating DSC thermograms of P(MMA/MA15) copolymers with different diameters.

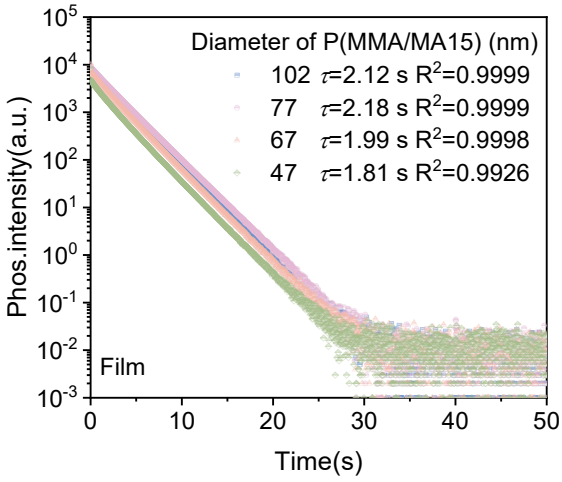

Fig. S13. Lifetime decay curve for the RTP emission peak of P(MMA/MA15) films with different diameters.

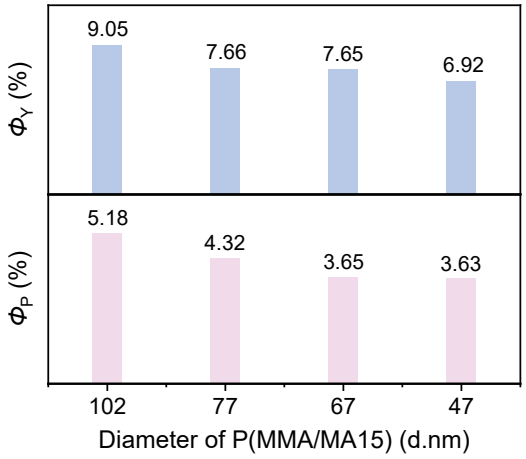

Fig. S14. Φ_{Yield} and Φ_{Phos} of P(MMA/MA15) films with different diameters.

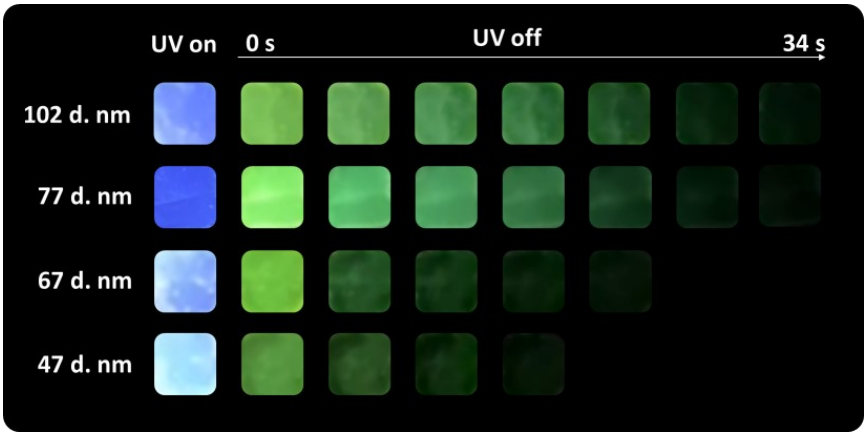

Fig. S15. Afterglow photos of P(MMA/MA15) films with four different diameters.

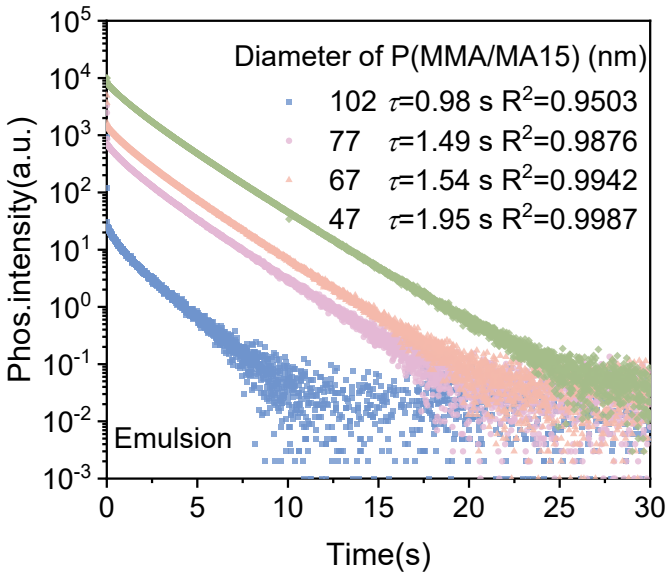

Fig. S16. Lifetime decay curve for the RTP emission peak of P(MMA/MA15) emulsions with different diameters.

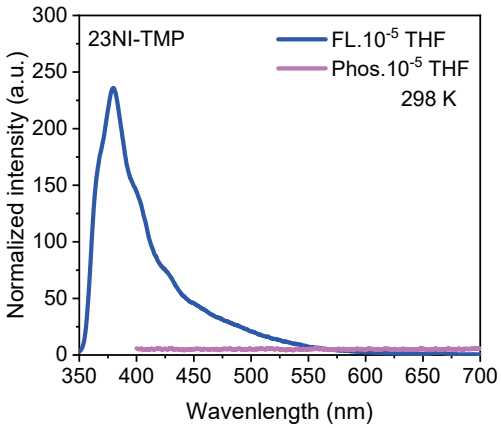

Fig. S17. Prompt and delayed PL spectra of 23NI-TMP (10^{-5} M) at room temperature.

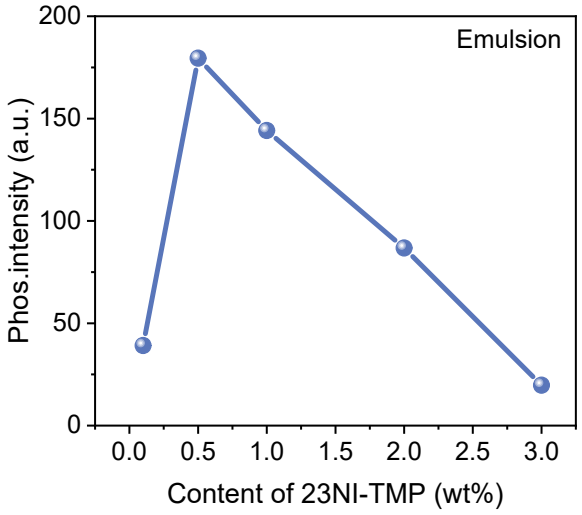

Fig. S18. Changes of phosphorescence intensity with the content of 23NI-TMP ranging from 0.1 wt% to 3.00 wt% in P(MMA/MA15) emulsion.

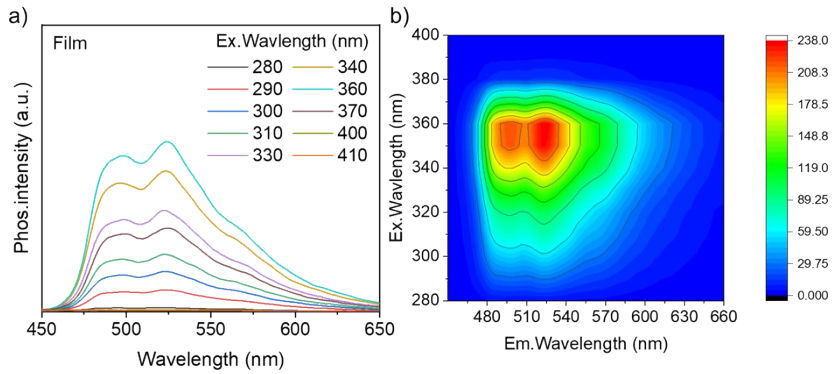

Fig. S19. a) Delayed PL spectra and b) phosphorescence-excitation mapping of 23NI-TMP@P(MMA/MA15) film from 310 to 400 nm (content of 23NI-TMP: 0.5 wt%).

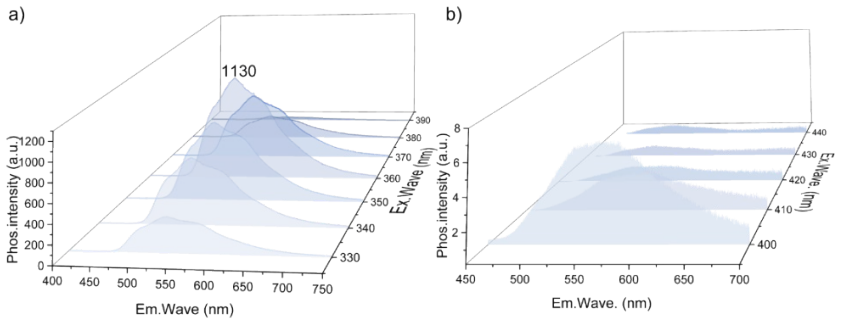

Fig. S20. Delayed PL spectra of 23NI-TMP@P(MMA/MA15) emulsion: a) under excitation from 330 to 390 nm, and b) under excitation from 400 to 440 nm (23NI-TMP content: 0.5 wt%).

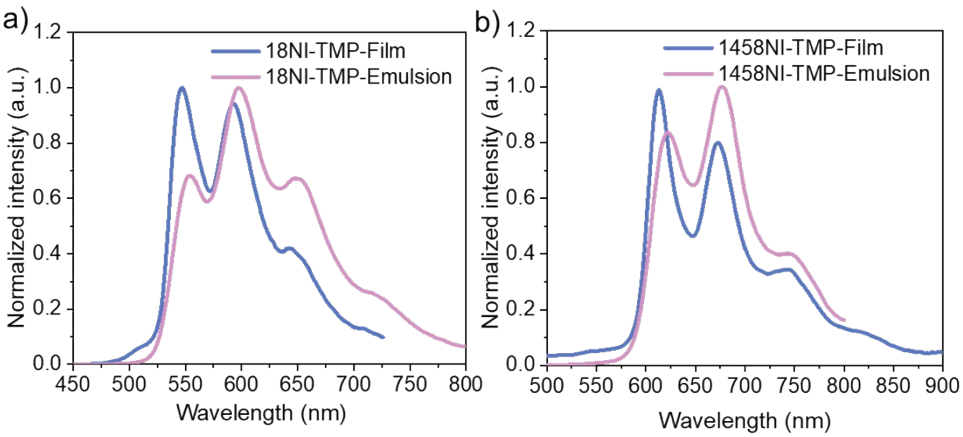

Fig. S21. Delayed PL spectra of film and emulsion of a) 18NI-TMP and b) 1458NI-TMP.

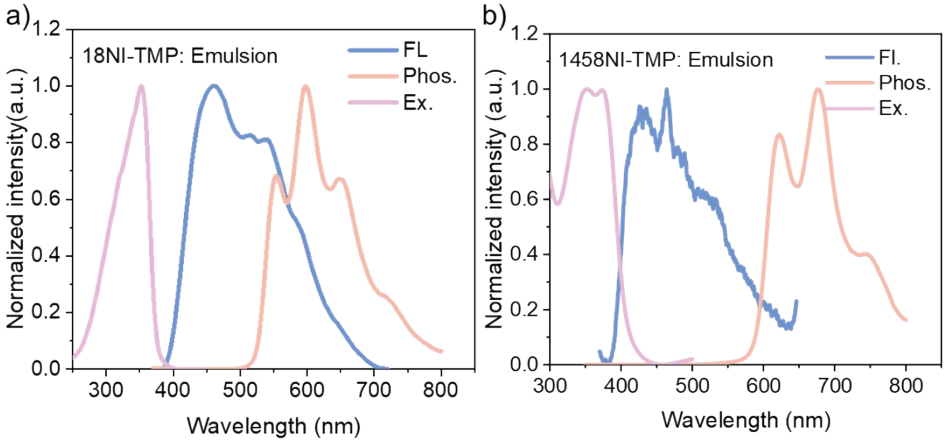

Fig. S22. Prompt, delayed and excitation spectra of a) 18NI-TMP@P(MMA/MA15) and b)1458NI-TMP@P(MMA/MA15).

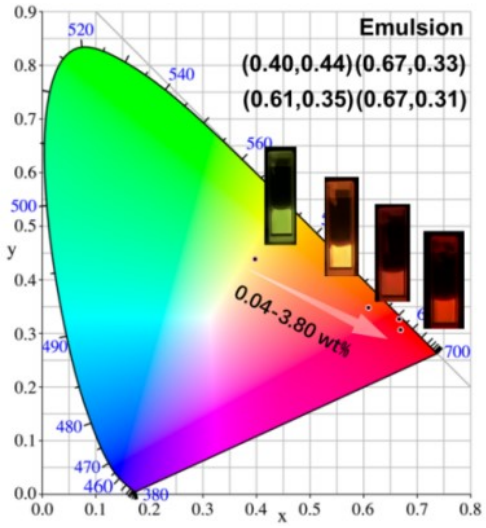

Fig. S23. Photos and CIE chromaticity diagram of S-P(MMA/MA15) emulsion after turning off the UV-365 nm excitation (content of Safr-T from 0.04 to 3.80 wt%).

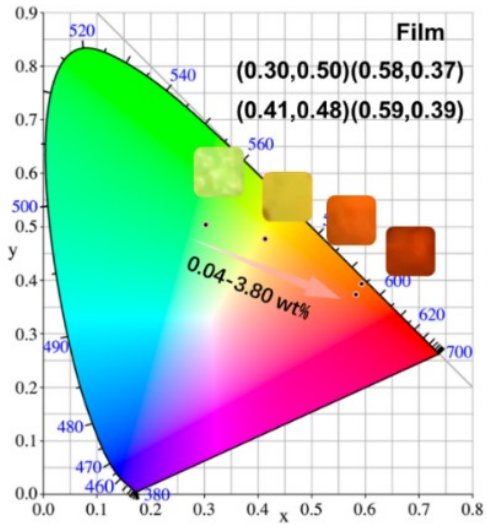

Fig. S24. Photos and CIE chromaticity diagram of S-P(MMA/MA15) film after turning off the UV-365 nm excitation (content of Safr-T are from 0.04 to 3.80 wt%).

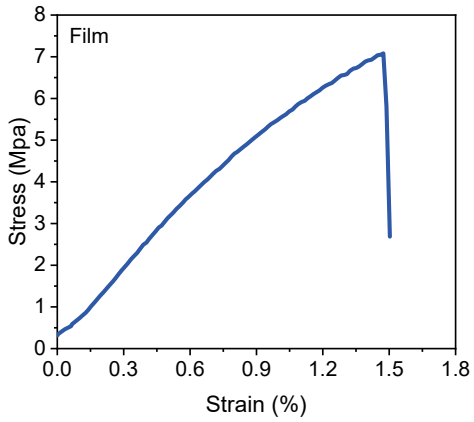

Fig. S25. Stress-strain curve of P(MMA/MA15) film.

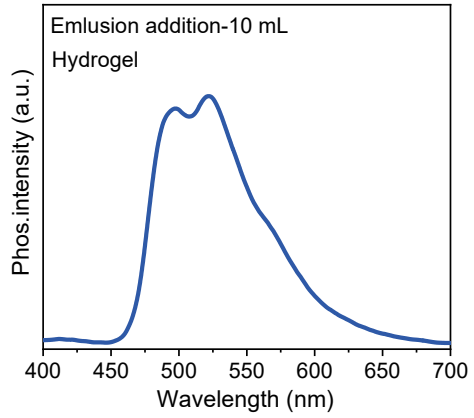

Fig. S26. Delayed PL spectra of P(MMA/MA15) hydrogel at 10 mL emulsion-added.

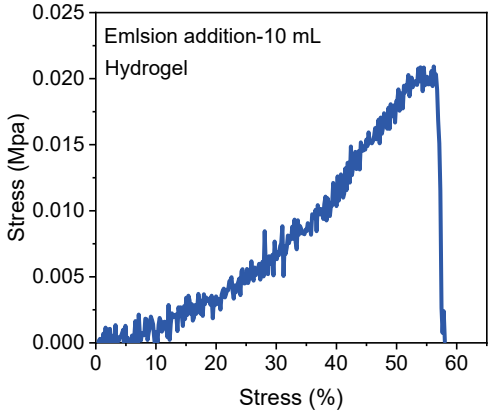

Fig. S27. Stress-strain curves of P(MMA/MA15) hydrogel at 10 mL emulsion-added.

References

1. C. Qian, Z. Ma, X. Fu, X. Zhang, Z. Li, H. Jin, M. Chen, H. Jiang, X. Jia and Z. Ma, *Adv. Mater.*, 2022, **34**, e2200544.
2. Z. Mao, G. Zhang, H. Ma, J. Liu, S. Xue, Q. Sun and W. Yang, *Dyes Pigm.*, 2025, **236**, 112679.
3. Z. Chen, J. Shi, Y. Zhou, P. Zhang and G. Liang, *Chin. Chem. Lett.*, 2025, **36**, 110629.
4. Y. Zhu, M. Pan, W. Ji, L. Ma, Y. Wang and L. Ruan, *Spectrochim. Acta A*, 2025, **330**, 125763.
5. X. Meng, Q. Hu, X. Wang, T. Ma, W. Liu, X. Zhu and C. Ye, *J. Mater. Chem. C*, 2022, **10**, 17620-17627.
6. C. Qian, X. Zhang, Z. Ma, X. Fu, Z. Li, H. Jin, M. Chen, H. Jiang and Z. Ma, *CCS Chem.*, 2024, **6**, 798-811.
7. S. Zhang, G. Liu, Z. Mao, S. Xue, Q. Sun and W. Yang, *Chem. Sci.*, 2024, **15**, 19886-19892.
8. H. Yao, F. Yang, J. Hu, W. Cao, S. Qin, T.-B. Wei, B. Shi and Q. Lin, *Chin. Chem. Lett.*, 2025, **36**, 110375.
9. Y. Zhang, Q. Sun, J. Chen, S. Cui, H. Zhang, S. Xue and W. Yang, *Chem. Eng. J.*, 2022, **447**, 137458.
10. X. Wang, X. Meng, T. Cui, Q. Hu, B. Jin, Y. He, X. Zhu and C. Ye, *Carbohydr. Polym.*, 2024, **341**, 122309.
11. Q. Wang, X. Liu, Y. Su, Y. Shi, K. Feng, L. Liu, W. Sun, Y. Dong, J. Ma and X. Chen, *Adv. Opt. Mater.*, 2025, **13**, 2500428.
12. X. Zheng, Q. Han, Q. Lin, C. Li, J. Jiang, Q. Guo, X. Ye, W. Z. Yuan, Y. Liu and X. Tao, *Mater. Horiz.* , 2023, **10**, 197-208.